STUDY ON THE INFLUENCE OF EVAPORATOR OF ORC SYSTEM ON ENGINE PERFORMANCE

Chen Bei[1,2]*, Hongguang Zhang[1,2]

[1]Beijing University of Technology, College of Environmental and Energy Engineering,
Beijing, China
E-mail: bc887410@126.com

[2]Collaborative Innovation Center of Electric Vehicles in Beijing,
Beijing, China
E-mail: bc887410@126.com

* Corresponding Author

ABSTRACT

In this paper, a simulation model of a fin-and-tube evaporator for the organic Rankine cycle (ORC) system is established by Fluent software. Then, the flow and heat transfer characteristics of the exhaust at the evaporator shell side are obtained, and then the performance of fin-and-tube evaporator of the ORC system is analyzed based on the aforementioned simulation results. Subsequently, the influence of evaporator of the ORC system on engine performance is studied. A simulation model of the engine is developed by using GT-Power under various operating conditions, the variation of engine power, torque and brake specific fuel consumption (BSFC) are obtained. Results show that, owing to the pressure drop caused by the evaporator of the ORC system, the diesel engine power and torque decreases slightly, while the BSFC increases slightly with the increase of exhaust back pressure. With the increase of engine speed, the power loss, the torque loss and the BSFC increment increase gradually, where the biggest change is less than 1%.

1. INTRODUCTION

With the development of economy, the car ownership is increasing rapidly; it will cause a lot of energy consumption and serious environmental pollution. Of the engine's fuel combustion energy, only about one third is converted into mechanical energy and the remaining is dissipated in the form of waste heat through the exhaust and the coolant system (Heywood JB, 1988).

Organic Rankine cycle (ORC) is an effective method for waste heat recovery and has been widely applied in many domains. Yari *et al*. (2011) investigated recovery waste heat from a gas turbine-modular helium reactor using different arrangements of organic Rankine cycles (ORCs) which included simple organic Rankine cycle, ORC with internal heat exchanger and regenerative organic Rankine cycle. The results showed that simple organic Rankine cycle is the best from the view of both thermodynamics and economics, the efficiency of this cycle was about 10% higher than that of without ORC system. Baik *et al*. (2012) proposed that the heat-transfer performance of the exchanger has a significant impact on the output power of the ORC. M. Hatami *et al*. (2014) recycled exhaust gas energy of gasoline engine and diesel engine by two different evaporators separately. The evaporators were simulated under three different kinds of turbulence model by Fluent software. Then, the variations of outlet temperature of exhaust and working fluid depended on the engine torque are obtained. The results showed that, simulation results which select the SST k-ω and RNG k-ε model are closer to experimental results. Borrajo-Pelaez R, *et al*. (2010) studied the performance of a plain fin-and-tube heat exchanger, and 3D numerical simulation method were used with higher heat transfer accuracy. Perrotin and Clodic (2004) presented the results of 2D and 3D CFD models of compact

louvered heat exchangers for the determination of heat transfer and pressure drop characteristics and local information analysis. 2D and 3D steady simulations were performed and compared to experimental results and correlations of the literature. J.F. Zhang *et al*. (2009) simulated the flow and heat transfer process of the spiral baffle plate heat exchanger shell side by Fluent software, and analyzed the mechanism of heat transfer use the field synergy principle. The results had a certain theoretical guiding significance for design the spiral baffle plate heat exchanger. Zhang *et al*. (2008) analyzed experimental and numerical heat transfer characteristics of a helically baffled heat exchanger combined with one three-dimensional finned tube. The results indicated that numerical investigations agree well with the measurements. Ozden *et al*. (2010) investigated the shell side design of a shell-and-tube heat exchanger by numerically modeling a small heat exchanger. The flow and temperature fields inside the shell were resolved using a commercial CFD package. The results showed that CFD simulations can pin point the source and the location of the weakness. Using CFD, together with supporting experiments, may speed up the shell-and-tube heat exchanger design process. Aytunc Erek *et al*. (2005) studied the influence of the geometric structure of the fin on heat transfer and resistance characteristics of heat exchanger based on the numerical simulation method use CFD software. The results showed that, the fin spacing has a considerable effect on the pressure drop. Therefore, taking as the heat transfer component of the ORC system, evaporator has an impact on ORC system, but also influences engine performance.

The main target of this research is to analyze the flow and heat transfer characteristics of the engine exhaust at the evaporator shell side and the influences of evaporator used in ORC system on engine performance under various operating conditions.

2. SIMULATION MODEL OF EVAPORATOR

2.1 Physical Model of Evaporator

In this paper, the flow and heat transfer characteristics of the exhaust at the evaporator shell side are obtained using Fluent software. The half section physical model of the fin-and-tube evaporator is shown in Fig.1. It consists of the front-end part, the main body, and the rear-end part. The main body is the heat convection place of the exhaust gas and the organic working fluid. The high temperature exhaust gas of diesel is at the evaporator shell side, the low temperature organic working fluid is in the tube side. The specific geometric parameters of fin-and-tube evaporator are shown in Table 1.

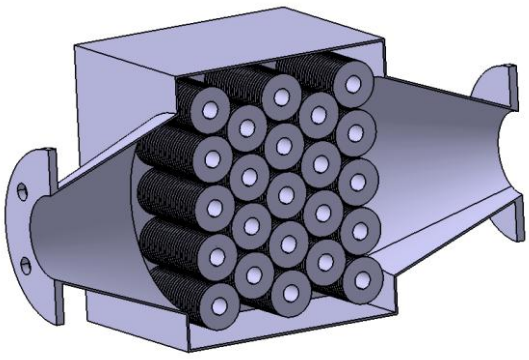

Figure 1: Physical model for the fin-and-tube evaporator

Table 1: Geometric dimensions of the fin-and-tube evaporator

Item	Parameter	Unit
Number of tube rows	5	-
Number of tubes in a row	4 or 5	-
Total number of tubes	23	-
Fin thickness	1	mm
Fin height	27	mm

Tube outside diameter	27	mm
Tube inner diameter	20	mm
Tube pitch	47×56	mm
Tube row alignment	Staggered	-

In order to ensure the accuracy of the flow and heat transfer calculation and simplify the numerical calculation, we used a quarter of the evaporator's physical model for calculations and make the following assumptions: (1) The thermal physical properties of the exhaust gas are set as constants based on the average exhaust temperature. (2) The temperatures of fins, round tubes and shells are set to average value. (3) The flow of exhaust gas at the evaporator shell side is turbulent, and the heat-transfer process is steady. (4) Ignore the free convection and gravity of the exhaust gas.

2.2 Boundary Conditions

In this paper, the fin-and-tube evaporator is used for recovery the exhaust heat of a diesel engine. We study the flow and heat transfer characteristics of the exhaust at the evaporator shell side at one steady operation point, where the engine speed is 2600 r/min and the engine torque is 180.7 N·m. According to the engine test data, mass flow rate of the intake air is 0.06464 kg/s, the fuel injection rate is 0.00324 kg/s and the exhaust temperature at the inlet of the evaporator is 628 K. Thus, the mass flow rate of the exhaust, which is the summation of the intake air and the injected fuel, is 0.06788 kg/s. The exhaust pressure at the outlet is set to the ambient pressure. The boundary conditions are summarized in Table 2. In this study, the thermodynamic properties of the exhaust gas are set as constants based on the average exhaust temperature.

Table 2: The boundary conditions

Item	Parameter	Unit
Mass flow rate of exhaust gas	0.06788	kg/s
Temperature at evaporator inlet	628	K
Pressure at evaporator outlet	1.01×10^5	Pa
Temperature of fins and tubes	450	K
temperature of shells	555	K

2.3 Grid Generation and Numerical Method

The geometry model of evaporator is established using CATIA software. We used a quarter of the evaporator's physical model for calculations based on the principle of symmetry. We built 3D grid system using the commercial tool ICEM 14.5 and discretized it with unstructured elements of tetra/mixed type. The grid of evaporator model is shown in Fig.2.

A careful check for the grid-independence of the numerical solutions has been made to ensure the accuracy and validity of the numerical results. In order to verify the independence of grid system, three different grid systems were obtained. The first grid system has 3,314,020 cells, the second grid system has 4,426,733 cells, and the last one has 5,901,946 cells. Through the simulation calculation, the exhaust temperatures at the outlet of the evaporator for three different grid systems were obtained. The relative errors of the average exhaust temperature at the outlet are 0.42% and 0.21%, respectively. Thus, the solution precision of the last grid system is satisfactory.

The numerical calculations are used for Fluent14.5. A finite volume method is employed to discrete the governing equations. The SIMPLE algorithm is selected in these numerical calculations. The convergence criteria are the residual errors is less than 10^{-3} for the velocity and the momentum equations and the residual errors is less than 10^{-6} for the residual error for the energy equation.

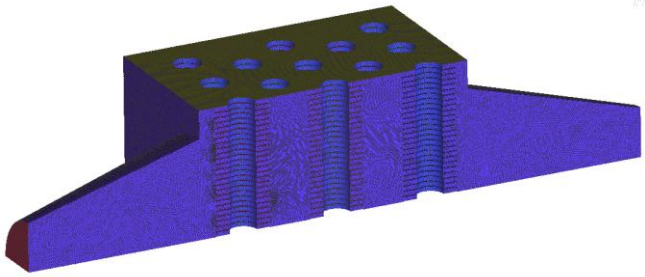

Figure 2: Grid of evaporator model

2.4 Results and Discussion of Evaporator Simulation

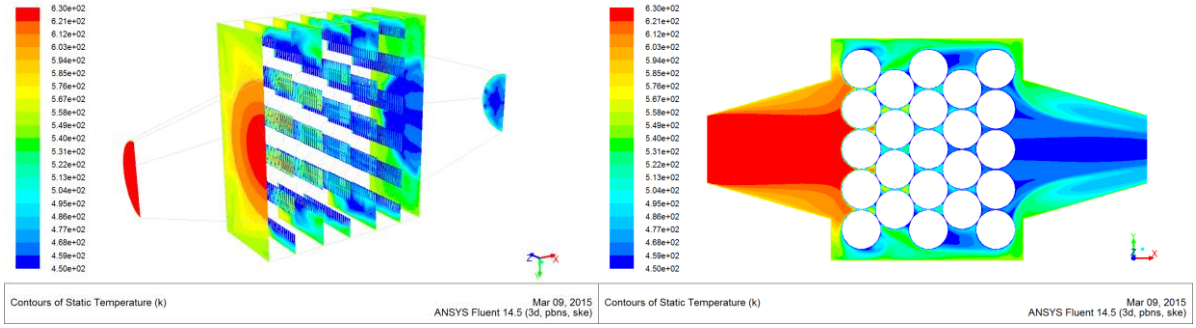

(a) Transversal surface section (b) Center symmetry section

Figure 3: Temperature distribution of exhaust in the evaporator

In order to analyze the flow and heat transfer characteristics of the exhaust at the evaporator shell side, we chose 9 planes in different positions vertical to the x-axis. The specific locations are shown in Fig.3 (a). The center symmetry plane vertical to the z-axis is shown in Fig.3 (b). To reduce the workload, we used a quarter of the evaporator's physical model for calculations. Afterwards, we symmetrize the results along the symmetric plane. We use 5 planes in the middle along the direction of the exhaust flow to represent the planes through the centerlines of the tube bundles in each row.

The details of the temperature distribution in the evaporator are shown in Fig.3. The exhaust temperature of the area of front-end part approximately equals the inlet exhaust temperature of 628 K. The exhaust temperatures of the two corners far from the central area are relatively lower at approximately 520 K. In addition, the flow areas of the high-temperature exhaust gas are nearly round and expand gradually along the flow direction. The exhaust temperatures of the round areas decrease gradually, which means the high-temperature exhaust gas in the flow space between the first and second rows diffuses quickly. The temperature of the exhaust gas near the fin is low, so the heat exchange efficiency is better.

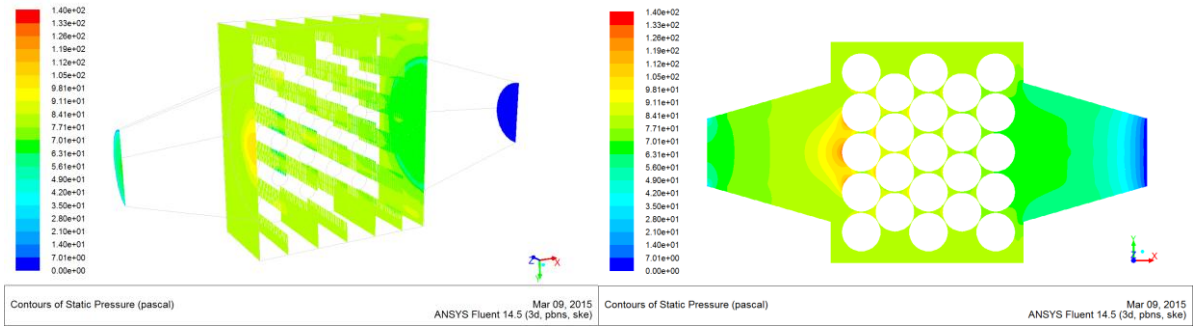

(a) Transversal surface section (b) Center symmetry section

Figure 4: Pressure distribution of exhaust in the evaporator

The details of the pressure distribution in the evaporator are shown in Fig.4. The maximum pressure of the evaporator exists on central area of the first row of the bundles near the front-end part. The high-temperature exhaust in the tapered divergent pipe is blocked by the tube bundles of the first row, rapidly reducing the exhaust mass flow rate, leading to a rapid increase of the exhaust pressure. The maximum pressure of the evaporator is 141.34 Pa and is significantly lower than the maximum limit of 30 kPa. The pressure drop of exhaust gas between import and export of evaporator is about 53 Pa. It is the back pressure of exhaust under this work point of diesel engine.

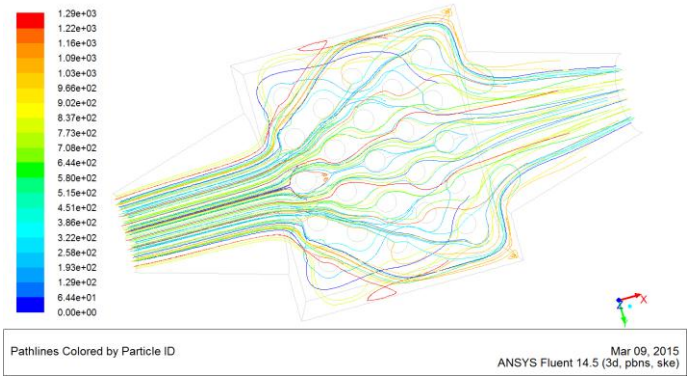

Figure 5: Streamlines of the exhaust gas in the evaporator

Streamlines of the exhaust gas in the evaporator are shown in Fig.5. The exhaust flow is well distributed, which means the convective heat transfer is fully developed in the center of the evaporator. In the two corners far from the center of the evaporator and near the front-end part, there little exhaust flow exists, resulting in a very poor convective heat transfer. However, the heat conduction process dominates in these regions and results in very low temperatures at the corners. Because the shape of the front-end part connecting with the main body is round, the exhaust flux entering into the main body is restricted in the domains close to the centers. The exhaust temperature of the central zones is quite low because of the cooling effects of the tube walls and the fins. Therefore, to ensure the exhaust flux is equally distributed in the spaces between the neighboring fin layers, the design of the shapes connecting the main body with the front-end and rear-end parts are very important.

According to the results of numerical simulation, the average exhaust temperature at the outlet of the evaporator is 473 K. The exhaust temperature is 491 K, according to the results of experiment. The error of the exhaust temperature at the outlet is 3.67 % which is in the reasonable scope. It verified the accuracy of the simulation mode. So the evaporator simulation model can be analyzed and researched. The reasons for error: only one point is measured for temperature sensor, but the result of numerical simulation is the average value in the face.

3. SIMULATION OF THE DIESEL ENGINE

3.1 Simulation Model of the Diesel Engine

In this paper BJ493ZLQ3 is selected as the research object. BJ493ZLQ3 is a diesel engine with inline four cylinders, four-stroke, forced water cooling, turbocharged intercooled, electronic control high pressure common rail. Technology parameters of the BJ493ZLQ3 diesel engine are showed in Table 3. A simulation model of the engine is developed based on GT-Power, the model includes: (1) The intake and exhaust system model. (2) Injector model. (3) Cylinder model. (4) Crankcase model. (5) Turbocharged system model. (6) The set of the system boundary conditions (temperature and pressure).

Table 3: Technology parameters of the BJ493ZLQ3 diesel engine

Item	Parameter	Unit
Cylinder diameter	93	mm
Stroke	102	mm
Compression ratio	17.4	-
Displacement	2.771	L
Rated power	85	kW
Rated speed	3600	r/min
Maximum torque	280	N·m
Speed at max. torque	2300	r/min

In this paper, the simulation model of BJ493ZLQ3 diesel engine is built, which is shown in Fig.6.

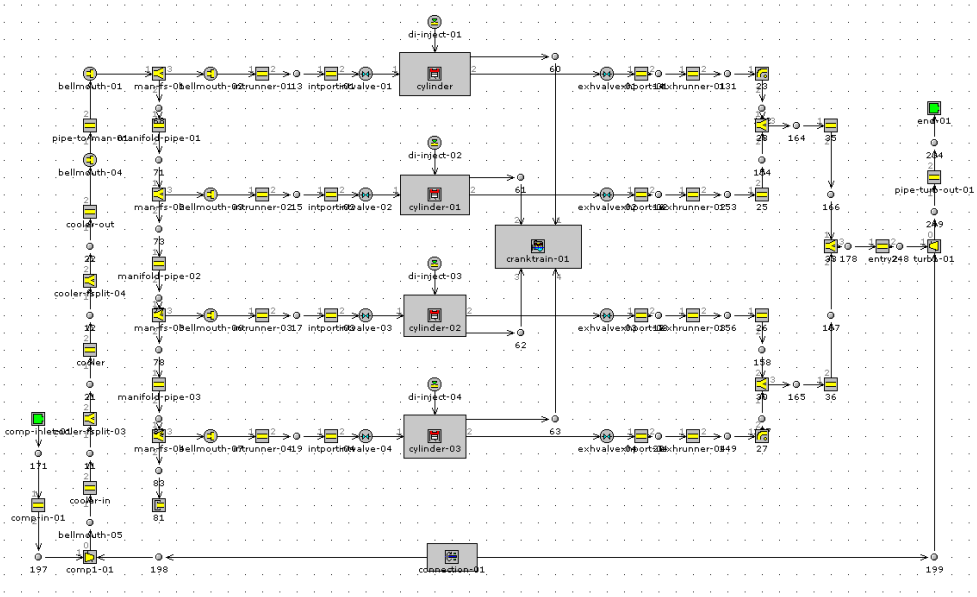

Figure 6: BJ493ZLQ3 diesel engine simulation model

3.2 Validation of Diesel engine Simulation Model

In order to ensure the simulation model can describe the actual operation of diesel engine and predict the performance of diesel engine effectively. The simulation results for various operating points are verified by using the experiment results of BJ493ZLQ3 diesel engine.

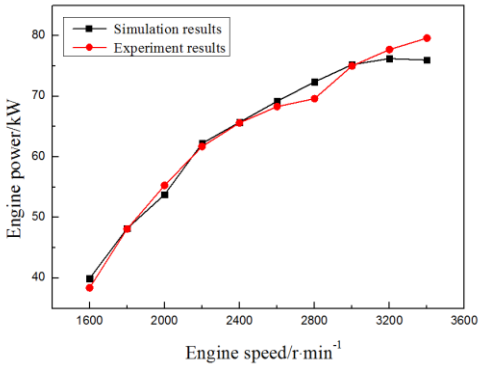

Figure 7: Simulation and experiment results of power at full load

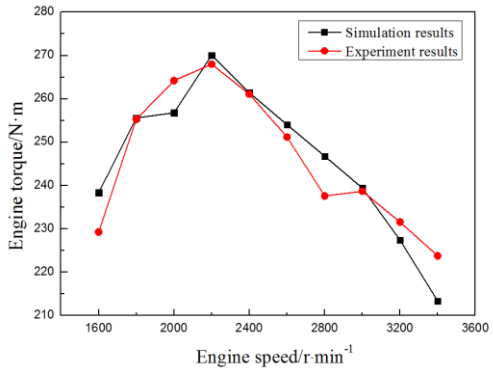

Figure 8: Simulation and experiment results of torque at full load

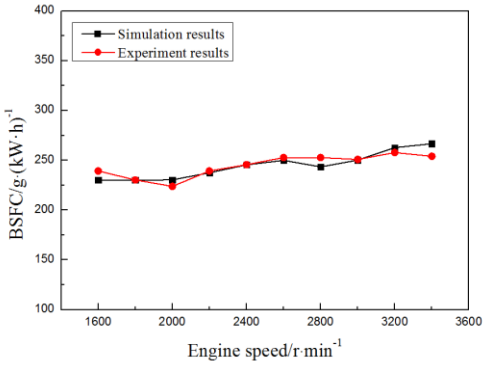

Figure 9: Simulation and experiment results of BSFC at full load

The simulation and experiment results of power, torque and brake specific fuel consumption (BSFC) of BJ493ZLQ3 diesel engine at full load are shown in Figures 7, 8 and 9. Simulation results have the similar variation trend with experiment results. At the speed of 3400 r/min, the relative error between simulation and experiment values of the power, torque and BSFC are all the biggest, which is 4.97%, 4.65% and 4.97% respectively.

According to the above-mentioned analysis, the maximum relative error between the simulation and experiment values is less than 5%. So, the engine simulation model can be employed with a high precision.

4. INFLUENCE OF EVAPORATOR ON THE ENGINE CHARACTERISTICS

In this study, the influence of evaporator of the ORC system on engine performance is studied under 6 operating conditions. The exhaust back pressure increment of engine exhaust is obtained according to the pressure drop between import and export of evaporator which is acquired from the simulation result. Then, a simulation model of the engine is developed by using GT-Power. The variation of engine power, torque and BSFC is discussed after equipping with evaporator of the ORC system under various operating conditions.

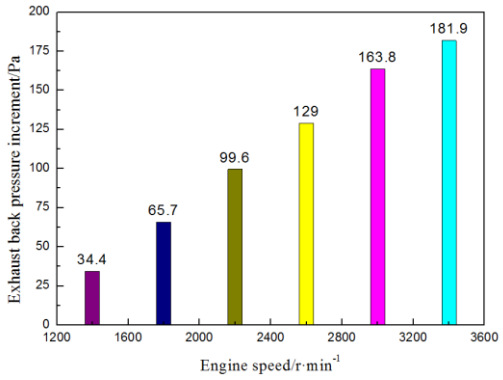

Figure 10: The exhaust back pressure increment of diesel engine under various operating conditions

The exhaust back pressure increment after equipping with evaporator of the ORC system under various operating conditions is shown in Fig.10. With the increase of engine speed, the engine exhaust back pressure increment increases gradually. The main reason is that, with the increase of engine speed, engine intake air mass flow rate increases gradually, which results in the increase of the exhaust mass flow rate, and then the pressure drop of engine exhaust increases at the evaporator shell side.

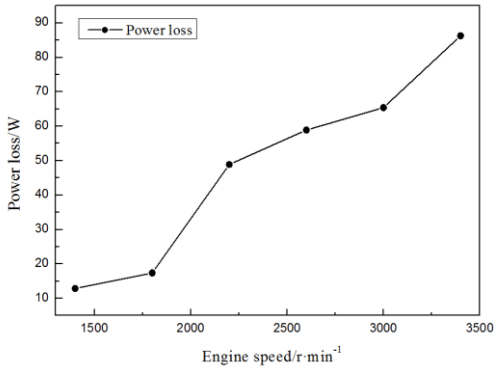

Figure 11: Power loss of diesel engine under various operating conditions

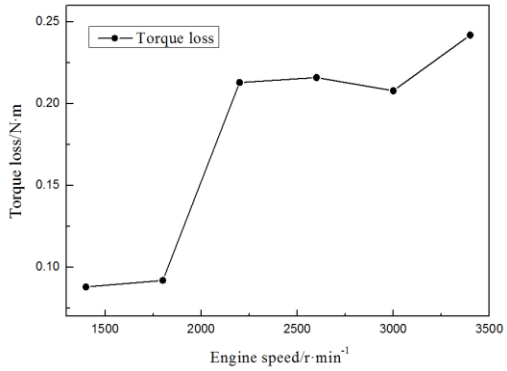

Figure 12: Torque loss of diesel engine under various operating conditions

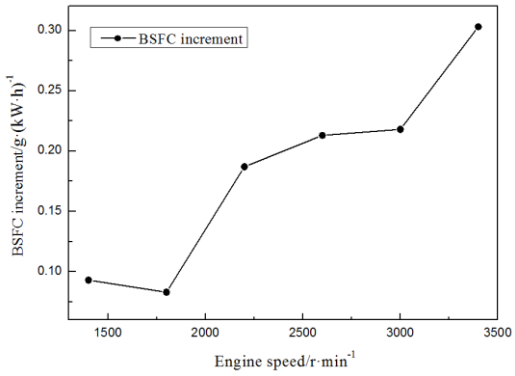

Figure 13: BSFC increment of diesel engine under various operating conditions

The power loss, the torque loss and the BSFC increment of diesel engine after equipping with evaporator of the ORC system under various operating conditions is shown in Fig.11-Fig.13. Equipped with the evaporator of the ORC system, the diesel engine power and torque decreases within a small range, while the BSFC increases within a small range with the increase of exhaust back pressure. With the increase of engine speed, the power loss, the torque loss and the BSFC increment of engine increase gradually. The main reason is that, diesel engine exhaust generated flow resistance in the shell side of evaporator after equipping with evaporator of the ORC system. Subsequently, exhaust back pressure of engine increased. With the increase of exhaust back pressure, residual gas pressure in cylinder of the diesel engine raised. This will not only increase the residual gas coefficient, furthermore, reduces the charging coefficient, but also increase the pumping loss. Finally, the engine power and torque decreased while the BSFC increased.

5. CONCLUSIONS

In this study, a simulation model of a fin-and-tube evaporator of an ORC system is established by Fluent software. Then, the flow and heat transfer characteristics of the exhaust at the evaporator shell side are obtained. Subsequently, the influence of evaporator of the ORC system on engine performance is studied.

- The exhaust gas temperatures decrease gradually along the flow direction at the evaporator shell side. The exhaust gas in the flow space between the first and second rows diffuses quickly. To ensure the exhaust flow is equally distributed in the spaces between the neighboring fin layers, the design of the shapes connecting the main body with the front-end and rear-end parts are very important.
- The maximum exhaust pressure occurs in the connection area between the front-end part and the main body because of the sudden reduction of the flow area. With the increase of engine speed, the engine exhaust back pressure increment increases gradually after equipping with evaporator of the ORC system.
- The diesel engine power and torque decreases within a small range, while the BSFC increases within a small range with the increase of exhaust back pressure after equipping with evaporator of the ORC system. With the increase of engine speed, the power loss, the torque loss and the BSFC increment of engine increase gradually.

REFERENCES

Heywood JB., 1988, Internal Combustion Engine Fundamentals, *McGraw-Hill*, New York, p.673-674.

Yari M., Mahmoudi S.M.S., 2011, A thermodynamic study of waste heat recovery from GT-MHR using organic Rankine cycles, *Heat Mass Transfer*, vol. 47: p.181–196.

Baik Y, Kim M, Chang K, Lee Y, Yoon H., 2012, Power enhancement potential of a mixture transcritical cycle for a low-temperature geothermal power generation, *Energy*, vol. 47: p.70–76.

Hatami M., Ganji D.D., Gorji-Bandpy M., 2014, Numerical study of finned type heat exchangers for ICEs exhaust waste heat recovery, *Case Studies in Thermal Engineering*, vol. 4: p.53–64.

Borrajo-Pelaez R., Ortega-Casanova J., Cejudo-Lopez J.M., 2010, A three-dimensional numerical study and comparison between the air side model and the airwater side model of a plain fin-and-tube heat exchanger, *Applied Thermal Engineering*, vol. 30: p.1608–1615.

Perrotin T, Clodic D., 2004, Thermal-hydraulic CFD study in louvered fin-and-flat-tube heat exchangers, *International Journal of Refrigeration*, vol. 27, no. 4: p.422–432

Zhang J.F., He Y.L., Tao W.Q., 2009, 3D numerical simulation on shell-and-tube heat exchangers with middle-overlapped helical baffles and continuous baffles - Numerical model and results of whole heat exchanger with middle-overlapped helical baffles, *International Journal of Heat and Mass Transfer*, vol.52: p.5371–5389.

Zhang Z.G., Ma D.B, Fang X.M., 2008, Experimental and numerical heat transfer in a helically baffled heat exchanger combined with one three-dimensional finned tube, *Chemical Engineering and Processing*, no. 47: p.1738–1743.

Ozden E., Tari I., 2010, Shell side CFD analysis of a small shell-and-tube heat exchanger, *Energy Conversion and Management*, vol. 51, no. 5: p.1004–1014.

Aytunc E., Bails O., Levent B., 2005, Effect of geometrical parameters on heat transfer and pressure drop characteristics of plate fin and tube heat exchangers, *Applied Thermal Engineering*, vol. 25, no. 14-15: p.2421-2431.

ACKNOWLEDGEMENT

This work was sponsored by the National Natural Science Foundation of China (Grant No. 51376011), the Beijing Natural Science Foundation Program (Grant No. 3152005), and the Scientific Research Key Program of Beijing Municipal Commission of Education (Grant No. KZ201410005003).